SANDIA REPORT

SAND96–2239 • UC–705
Unlimited Release
Printed September 1996

Oblique Penetration Modeling and Correlation with Field Tests into a Soil Target

Donald B. Longcope, Jr.

Prepared by
Sandia National Laboratories
Albuquerque, New Mexico 87185 and Livermore, California 94550
for the United States Department of Energy
under Contract DE-AC04-94AL85000

Issued by Sandia National Laboratories, operated for the United States Department of Energy by Sandia Corporation.

Available to DOE and DOE contractors from
Office of Scientific and Technical Information
PO Box 62
Oak Ridge, TN 37831

Prices available from (615) 576-8401, FTS 626-8401

Available to the public from
National Technical Information Service
US Department of Commerce
5285 Port Royal Rd
Springfield, VA 22161

NTIS price codes
Printed copy: A03
Microfiche copy: A01

SAND96-2239
Unlimited Release
Printed September 1996

Distribution
Category UC-705

Oblique Penetration Modeling and Correlation with Field Tests into a Soil Target

Donald B. Longcope, Jr.
Structural Dynamics Department, 9234
Sandia National Laboratories
Albuquerque, New Mexico 87185-0439

Abstract

An oblique penetration modeling procedure is evaluated by correlation with onboard acceleration data from a series of six penetration tests into Antelope Dry Lake soil at Tonopah Test Range, Nevada. The modeling represents both the loading which is coupled to the penetrator bending and the penetrator structure including connections between the major subsections. Model results show reasonable agreement with the data which validates the modeling procedure within a modest uncertainity related to accelerometer clipping and rattling of the telemetry package. The experimental and analytical results provide design guidance for the location and lateral restraint of components to reduce their shock environment.

Acknowledgements

The author thanks Ron Lundgren, Department 9811, for discussions regarding the field measurements and data processing, Mike Forrestal, Department 9811, for discussions on the specification of soil properties for the cavity expansion load model, Dave Ryerson, Department 2664, for information about the on-board data filtering procedures, and Ned Hansen, Department 2165, for project support and helpful discussions on implications of the results for improved component packaging.

Table of Contents

Figures

Tables

Oblique Penetration Modeling and Correlation with Field Tests into a Soil Target

Introduction

Methods of understanding and predicting penetration into concrete and geologic targets can be classified as empirical, approximate engineering, or detailed numerical and may focus on trajectories, penetrator structural response, or the shock environment experienced by penetrator components. Empirical approaches may require extensive data bases, while rigorous numerical approaches, which couple an Eulerian target representation to a Lagragian penetrator description, may be limited in scope or require long computer processing time. Figure 1 shows a typical oblique penetration event in which, if either the angle of attack α or the angle of impact β are not zero, the motion of both the penetrator and target will be three dimensional. Reference [1] developed a predictive engineering procedure to determine the coupled lateral loading / penetrator bending and showed good agreement of model results with measured lateral accelerations for one field test of a Pershing II penetrator into antelope tuff, a soft dry rock. Ref. [2] describes a series of normal and oblique penetration tests into a well characterized soil target at the Sandia Tonopah Test Range, Nevada. The on-board acceleration data from these tests, Ref.[3], has shown excellent agreement with the axial rigid body acceleration calculated from the cavity expansion load model of Ref. [2], which provided validation of that model.

In the present work, modeling results based on the procedure of Ref. [1] are compared to the lateral and axial acceleration data of Ref.[3] to seek additional validation of the lateral load modeling procedure. The modeling results incorporate a structural model of the penetrator which is flexible in the axial and lateral directions and addresses the connections between the major penetrator subsections (case, ballast, and telemetry package). An evaluation of the lateral data is given which considers the determination of penetrator impact conditions and the accelerometer response and mounting. Results are given which provide design guidance in reducing the shock environment to components.

Structural Model of MOU Penetrator

A cross-section of the MOU peneatrator is shown in Fig. 2. The major components are the case, ballast, and telemetry package which weigh 30 lb., 14 lb., and 7 lb., respectively. An ABAQUS, Ref.[4], structural model is developed with the goal of adequately representing the acceleration histories at the forward and aft accelerometer locations. B21 beam elements are used with a pipe cross-section of constant outer radius equal to the average of

the radii at the ends of the element. These are two-node elements which represent bending, axial extension, and shear deformation, but no cross-sectional deformations. The structural model is shown in Fig. 2. All the nodes lie on the penetrator axis and are shown in the correctly scaled axial positions, but offset in the normal direction to allow visualization.

The case and ballast are made of steel with a Young's modulus of 30×10^6 psi, Poisson's ratio of 0.3, and density of 7.29×10^{-4} lb.-s^2/in.^{4}. The disks at the forward ends of the ballast and telemetry package are vulcanized rubber, assumed to have a Young's modulus of 2.56×10^4 psi, Poisson's ratio of 0.30, and density of 4.72×10^{-4} lb.-s^2/in.^{4}. The telemetry package consists of a steel cylindrical shell over most of the length which contains the electronics surrounded by potting material and steel housings at either end to which the accelerometers are attached with screws. The potting material and electronics together weigh 4 lb. and were modeled as a distributed mass without stiffness by increasing the density of the elements of the steel shell (2 lb.) to 20.6×10^{-4} lb.-s^2/in.^{4}.

During assembly, the telemetry package was inserted into the ballast cavity and compressed against the rubber disk at the forward end with a force of 1,000 lb. until the locking ring was secured to maintain the compression. Then the ballast was inserted into the case cavity and compressed against the rubber disk at the forward end until the aft end of the ballast was seated against a ledge in the case. A locking ring at the aft end was secured to maintain the compression. During soil penetration, the penetrator deceleration acts to increase the compression between the aft end of the ballast and the ledge of the case. The aft connection between the ballast and case is modeled as a rigid connection between node 13 of the case and node 24 of the ballast. The ballast, near its forward end, is connected to the case through the compressed rubber disk, represented by an element with nodes 5 and 16. The stiffening rings of the ballast have intermittrnt contact with the inside surface of the case across a radial gap, which is required for assembly. This interaction is modeled by the extremes of either a rigid connection or no connection at all between neighboring nodes of the case and ballast.

Typical penetration decelerations are more than sufficient to relieve the compression between the aft end of the telemetry package and the locking ring. Since this occurs at about 140 g, the aft end is free during most of the penetration event and can rattle in the radial gap between the telemetry package and the inside surface of the ballast. This is represented by a nonlinear spring, defined in Table 1, between nodes 22 and 33 that has very low stiffness to model motion in the gap and high stiffness to model the contact between the telemetry package and the ballast. It was deemed not practical to model the localized, intermittent contact between the telemetry package and the ballast, since the associated time scale would be very short compared to the lowest bending mode response of the penetrator. It is assumed that the only other ballast/telemetry package interaction is at the forward end of the telemetry package through the compressed rubber disk and a very stiff spring between nodes 16 and 27 which models possible contact.

The response of the accelerometers depends significantly on the restraint of the ballast and telemetry package. In the calculations, two cases were considered -- one of limited restraint

BC1 through the previously defined rubber disks and nonlinear springs, which approximates the actual MOU penetrator, and one of perfect restraint BC2 in which the nodes across the rubber disks, across the nonlinear spring, and between the coincident nodes of the case and ballast were assumed to be rigidly connected. The rigid connections generally produced a lower amplitude acceleration, particularly in the lateral direction, at both the forward and aft accelerometer locations than did the more "realistic", compliant connections.

Correlation of Penetrator Structural Model with Laboratory Modal Tests

Laboratory modal tests of the MOU penetrator consisting of the case, ballast and telemetry package were conducted at both low and high amplitude levels by Mayes, Refs.[5,6]. The penetrator was suspended with elastic cords. A fitting attached to the nose was impacted with a hammer in the low amplitude test and with a reverse Hopkinson bar fired from an air gun in the high ampliltude test. The high amplitude test achieved levels of 5,000 g, which were comparable to expected field test levels. The best defined modes and frequencies were the lowest bending and axial case modes obtained in the low amplitude test and listed in Table 2. Other internal modes detected in the low amplitude test were poorly defined and highly damped. Determination of the modes in the high amplitude test was more difficult and the results more uncertain due to observed nonlinear effects such as rattling and amplitude dependence and the lowest case bending and axial modes show some difference, Table 2, with those of the low amplitude test. An important result of the high amplitude tests was that accelerometers mounted on the case showed significant differences in response with the accelerometers of the telemetry package at the same axial locations. This indicates a need to model the ballast and telemetry package as well as the case in developing a structural model of the MOU penetrator for correlating with the field tests into soil.

An ABAQUS structural model which closely approximates that of Fig. 2 was solved for the lowest few bending and axial natural frequencies which are listed in Table 2. In the model, the ballast is rigidly connected to the case at the aft end and unconnected at the forward end, while the telemetry package is rigidly connected to the ballast at both ends. These connections adequately approximate those of the realistic connections BC1 for the purpose of determining the lowest case frequencies, which were not sensitive to these connections. Although the penetrator deceleration in the field tests was sufficient to release the aft end of the telemetry package, this condition was not duplicated in the laboratory modal testing. The model frequencies are in substantial agreement with the few test frequencies that were obtained, which provides a partial validation of the structural model.

Soil Model and Distributed Loading on Penetrator

The distributed axial and lateral loading on the penetrator were defined by using the DLOAD subroutine developed in Ref. [1] with specifications which represented the penetrator geometry of Fig. 2, test impact conditions, and soil model of Ref. [2]. Using either spherical or cylindrical cavity expansion results, the subroutine gives the distributed loads on an element which depend on its nodal velocities and rotations and on the geometry of a frustum with end radii equal to the outer radii of the penetrator cross-sections at the ends of the element.

The soil model is elastic-plastic with the plastic region being described by a constant, Tresca yield strength and a locking hydrostat and the elastic region being incompressible. Average values of the soil parameters used in the calculations are an initial density of 1.74×10^{-4} lb-s^2/in^4, a shear strength of 1.45×10^3 psi, a locking volumetric strain of 0.13, and a Young's modulus of 2.32×10^5 psi. These values represent averages of three cores through three soil layers, taken in the middle of the group of six penetration tests. Ref. [2] shows that the locking strain and Young's modulus are "weak" parameters in affecting the penetrator axial deceleration. The radial stress to expand either a spherical or cylindrical cavity with radial velocity for the specified soil parameters is given in Fig. 3. The spherical cavity expansion results were used to specify the distributed loading on the penetrator nose while the cylindrical cavity expansion results were used for the loading on the cylindrical aft-body. The use of the one-dimensional cavity expansion results to specify the axial and lateral penetrator loading is described in Ref. [1]. The spherical cavity expansion stress is identified as the stress normal to the penetrator surface while the cylindrical cavity expansion stress is taken as the stress at the penetrator surface in a radial direction normal to the penetrator axis. As in Ref. [2], sliding frictional forces at the penetrator surface are neglected because the soil had a water content of approximately 20 per cent and no erosion of the nose was observed.

Comparison of Model and Measured Accelerations

Soil Penetration Tests. In July 1990, six penetration tests, Table 3, were conducted into Antelope Dry Lake at Tonopah Test Range, Nevada. A mobile, 6.0 in., smooth-bore gas gun, Ref. [7], was used to propel the projectile shown in Fig. 2. An on-board recording package stored data from two, triaxial accelerometers at forward and aft locations, Fig. 2. The data was stored on-board after being processed by a 3,500 Hz low-pass, analog filter, Ref. [3].

Reference [2] compared predicted, axial, rigid-body deceleration histories with the accelerometer data filtered with a one kHz low-pass filter and found excellent agreement for all the tests except No. 1. In the correlation, the same soil model and parameter values presented herein were used. The data showed a modest oscillation with a dominant frequency about the predicted deceleration of the assumed-rigid penetrator.

In the present work, we will compare acceleration results of the penetrator structural model with lateral and axial accelerometer data for the oblique tests No. 3 and No. 5, which are essentially duplicates of No. 4 and No. 6. As shown in Fig. 4, test No. 3 was conducted at an angle of impact (obliquity) of 30 degrees and an angle of attack (yaw) of zero degrees, while No. 5 was at an angle of impact of zero degrees and an angle of attack of 3.5 degrees.

Evaluation of Data. In each test, the impact velocity V, angle of attack α, and angle of impact β, were determined from streak and framing camera data. Triaxial on-board acceleromters at the forward and aft ends recorded acceleration histories in the gun barrel and target in the X,Y, and Z directions, Fig. 4. The X and Y directions are the axial and lateral directions in the intended plane of the penetrator trajectory. The signals were filtered with a 3,500 Hz low-pass analog filter before being digitized at 23,675 samples/sec. and stored on-board. Endevco 7270A-6K piezoresistive accelerometers were used with a calibration of + 3,000/-3,000 g in the axial direction and +1,000/-1,000 g in the other directions.

The axial data were all consistent from the accelerometers in the forward and aft locations in both Tests 3 and 5, as shown in Figs. 5a and 8a. This data was also filtered with a 1,000 Hz, low-pass, 4-th order, Butterworth filter in MATLAB, Ref. [8]. The purpose of this was to afford a clearer comparison between data and model results and to show agreement of the present modeling with that of Ref. [2]. Figures 5b and 8b show the 1000 Hz data is consistent and possesses a dominant frequency.

The lateral data was consistent between duplicate tests, but shows significant clipping at the +/- 1,000 g levels, Figs. 6,7,9,and 10. This data was not filtered to 1,000 Hz because the clipping would no longer be apparent.

The intended angle of attack for Test No. 5 was 4.0 degrees. Since this relatively small angle produced a significant lateral acceleration, the experimental determination of α is evaluated. The penetrator was initially placed in the gun barrel at a 4.0 degree angle of attack with an error of +/- 0.25 degrees, Ref. [9], using bore riders forward and aft to maintain this angle in the gun barrel. The angle of attack was measured at 3.5 degrees with an estimated error of +/- 0.5 degrees just before impact with the soil surface using framing and streak cameras. A final determination of angle of attack was made by integrating with Simpson's rule in MATLAB the forward and aft X and Y accelerometers to get the penetrator X and Y components of velocity at exit from the gun barrel. The forward accelerometers gave α = 3.9 degrees while the aft accelerometers gave α = 3.7 degrees which are within the uncertainity of the photographic measurement. Finally, the photographic results showed that a stripe painted along the side from nose to tail of the penetrator did not rotate from gun barrel exit to target impact, indicating that the axial and lateral forces caused by the angle of attack would be in the plane defined by the X and Y accelerometer directions. The agreement of the angle of attack from the integration of the accelerometers with the photographic results is one indication that cross-axis sensitivity of the Endevco 7270A accelerometers was not significant.

Test No. 5 shows, at the aft end, a significant early lateral acceleration in a direction opposite to that of the lateral loading, Fig. 10. Initially, this was thought to be an anomalous result, which may have been caused by impact of the aluminum pusher plate which was located between the penetrator and compressed air in the gun barrel and followed the penetrator out of the gun. Analytical modeling results, presented later, agreed with this experimental response and showed that it is related to the lack of sufficient lateral restraint or looseness of the ballast and telemetry package.

ABAQUS Solution Procedures. An implicit dynamic solution procedure with a controlled time step was used for the solution. The NLGEOM option was chosen to allow possible large rotations and small strains of the penetrator beam elements. Other sources of nonlinearity include the coupling of the loading to the penetrator element orientation and nodal velocities and the nonlinear relation between cavity expansion velocity and loading, Fig. 3. The DLOAD subroutine makes use of ABAQUS internal variables describing the nodal motions and these required an update from the ABAQUS Version 4.8 used in Ref. [1] to Version 5.5 used for the present study. Typical solutions over about half a penetration event required 25 minutes of Cray J90 cpu time.

Comparison of Model and Test Accelerations. ABAQUS solutions were obtained for the penetrator model of Fig. 2 with each of the sets of restraint conditions, BC1 and BC2 under the impact conditions of Tests No. 3 and 5, Table 3. Axial and lateral accelerations at the forward and aft accelerometer locations were generated at 2.0×10^{-5} second time intervals. To approximate the 3500 Hz low-pass analog filtering of the data, the MATLAB Signal Processing Toolbox software, Ref. [8], was used to filter the model results with a 4th order, low pass, digital Butterworth filter with a 3,500 Hz cut-off frequency nondimensionalized by a Nyquist frequency equal to twice the solution sample rate. Both forward and reverse filtering were done to eliminate phase shifting. The axial acceleration results were additionally filtered with the same filter with a 1,000 Hz cut-off frequency.

Test No. 3 had an impact velocity of 912 ft./s, an angle of attack of zero degrees, and an angle of impact of 30 degrees. Comparisons of the measured and calculated axial accelerations at the forward accelerometer after low-pass filtering of 3,500 Hz and 1,000 Hz are shown in Figs. 5a and 5b, respectively. The comparisons show good agreement in general and excellent agreement of the rigid body acceleration (BC2) with the data filtered at 1,000 Hz, Fig. 5b, as was characteristic of the results of Ref. [2]. The data were filtered with the same filter as the model results except that a different Nyquist frequency corresponding to a data sample rate of 23,675 s^{-1} was used. The dominant frequency of about 800 Hz evident in the BC1 (compliant connection) results of Fig. 5b is a result of the telemetry package and rubber disk at its forward end acting like a one degree of freedom spring-mass system. The value of a Young's modulus for the nonlinear rubber was chosen to achieve this correlation. The lateral acceleration at the forward accelerometer showed only minor clipping of the data and reasonable correlation of the response amplitude with the BC1 and BC2 results, Figs. 6a,b. At the aft accelerometer location, the clipping is significant (especially between 0.005 and 0.006 seconds) and the BC1 results agree reasonably well in amplitude with the estimated data beyond the clipped region, Fig. 7a.

Generally, the aft acceleration amplitude is significantly higher, about a factor of two, than the forward amplitude. The set of rigid restraints, BC2, generally gave a lower amplitude response, both forward and aft, than the data and represents a possible design goal.

In Test No. 5 the penetrator had an impact velocity of 917 ft./s at an angle of attack of 3.5 degrees and an angle of impact of zero degrees. The impact velocity component normal to the penetrator axis was 56 ft./s in the positive x direction of Fig. 4. As for Test No. 3, the filtered model axial acceleration results for restraints BC1 and BC2 showed good agreement with the forward accelerometer data, Figs. 8a,b, and the same characteristic frequency of approximately 800 Hz. The forward lateral acceleration data is significantly clipped, but a projection beyond the clipped level shows reasonable amplitude agreement with the model results, particularly those with BC2. The aft lateral accelerometer data is severely clipped and actual amplitudes could be a factor of two higher than the clipped amplitudes. The model amplitudes for the perfect restraint BC2 appear to approximate data amplitudes projected beyond the clipping, Fig. 10b, while the results for the flexible restraint BC1 agree with the phasing of the data and show a substantial acceleration opposite in direction to the initial lateral loading. The three peaks of the calculated acceleration (not shown) are approximately +/- 5,000 g. As in Test No. 3, the aft lateral amplitudes are significantly greater than the forward ones and the perfect restraint condition BC2 gives a possible minimum amplitude response, both forward and aft, and represents a design goal.

Conclusion

(1) The cavity expansion-based procedure of Ref. [1] for modeling the coupled lateral loading and bending response of penetrators after oblique impact has been validated within a modest uncertainity for a class of soil targets exemplified by the Antelope Dry Lake test site at Tonopah Test Range, Nevada. This was achieved by an evaluation that confirmed the validity of lateral acceleration data from a set of penetration tests in the soil target except for some clipping of the accelerometer response; by demonstrating excellent agreement between data and model rigid body axial acceleration; and by demonstrating reasonable agreement between calculated and measured lateral acceleration amplitudes within the uncertainty of the data clipping and lateral rattling of the telemetry package, which was not amenable to modeling.

(2) The penetrator aft lateral acceleration is significantly higher (possibly a factor of two) than the lateral acceleration in the nose region, as demonstrated by both modeling results and measurements. This provides guidance in the location of sensitive components in penetrator systems.

(3) The flexible or loose lateral restraint set BC1, which approximates the restraints of the ballast and telemetry package within the test penetrator, resulted in significantly higher lateral accelerations than did the tied-contact restraint set BC2. This indicates that sufficient lateral restraint should be a design goal to minimize the shock environment in penetrators.

(4) Rattling of the telemetry package, characterized by free motion and local impact, due to insufficient lateral restraint is not amenable to modeling and was the cause of a major uncertainty in the model-test agreement. This indicates a need for a structural analyst to be closely coupled to a penetrator designer to achieve a modelable design for which performance can be predicted with acceptable accuracy.

References

[1]Longcope, D. B., "Coupled Bending / Lateral Load Modeling of Earth Penetrators, SAND-0789, Sandia National Laboratories, Albuquerque, NM, June, 1991.

[2]Forrestal, M. J. and Luk, V. K., "Penetration into Soil Targets," International Journal of Solids and Structures," Vol. 13, No. 3, pp427-444, 1992.

[3]Wood, W. R., "MOU Penetrator Acceleration Data, Test Numbers MOU 65-70," Sandia National Laboratories Test Reports, July 1990.

[4]ABAQUS/Standard User's Manual, Version 5.5, Vols. I and II, Hibbet, Karlsson, Sorensen, Inc., Providence, RI, 1995.

[5]Mayes, R. L., 7543, "Low-Level MOU Penetrator Modal Test," internal memo, Sandia National Laboratories, Albuquerque, NM, Sept. 19, 1990.

[6]Mayes, R.L., 7543, "High-Level MOU Modal Test," internal memo, Sandia National Laboratories, Albuquerque, NM, July 15, 1991.

[7]Lundgren R. G., Hightower, M. M., and Christensen, B.K., "Development of a Mobile Gas Gun," Proceedings of the 39 th Aeroballistic Range Association, Vol. 2, 1988.

[8]Little, J. N. and Shure, L., "Signal Processing Toolbox for Use with MATLAB," The Math Works, Inc., Natick, Mass., July, 1992.

[9]Lundgren, R. G., private communication, Dept. 9123, Sandia National Laboratories, Albuquerque, NM, Oct., 1992.

Table 1.Force versus Relative Displacement for Spring Elements

Spring Element Nodes	Relative Displacement(in.)	Force (in.)
n16/n27	-1.0	-390,000.
	-0.0085	-0.553
	0.0085	0.553
	1.0	390,000.
n22/n32	-1.0	-2,000.
	-0.0170	-0.20
	0.0170	0.20
	1.0	2,000.

Table 2.Modal Frequencies of the MOU Penetrator

Model (Hz)	Low Amplitude Test (hz)	High-Amplitude Test (Hz)	Mode
1,029	1,023	920	1st case bending
2,514	2,176	2,642	2nd case bending
3,474	3,544	3,664	1st case axial

Table 3.Soil Penetration Tests

Test Number	Impact Velocity (ft./sec.)	Angle of Attack (deg.)	Angle of Impact (deg.)
1	919	0	0
2	919	0	0
3	912	0	30
4	919	0	30
5	917	3.5	0
6	919	4.0	0

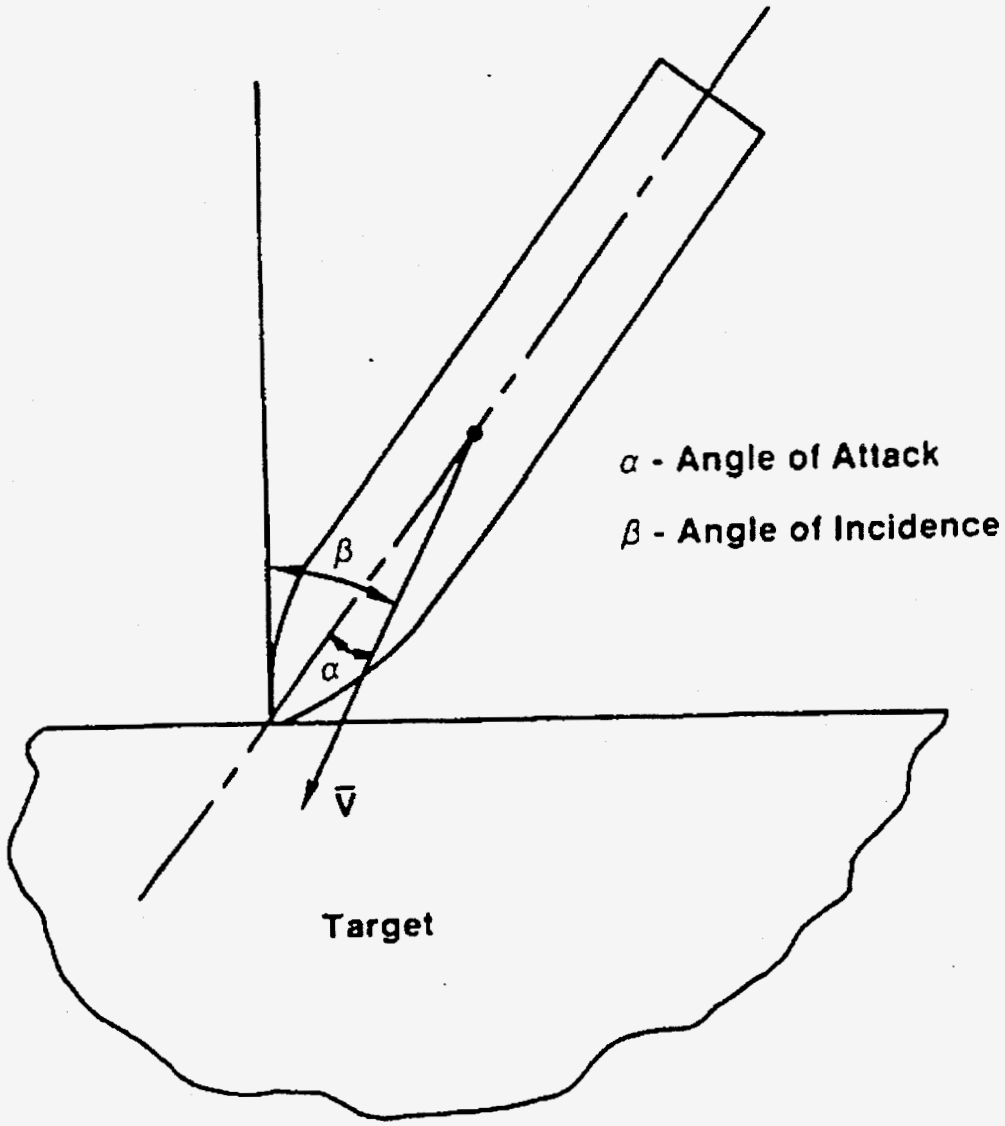

Figure 1. Geometry of an Oblique Impact

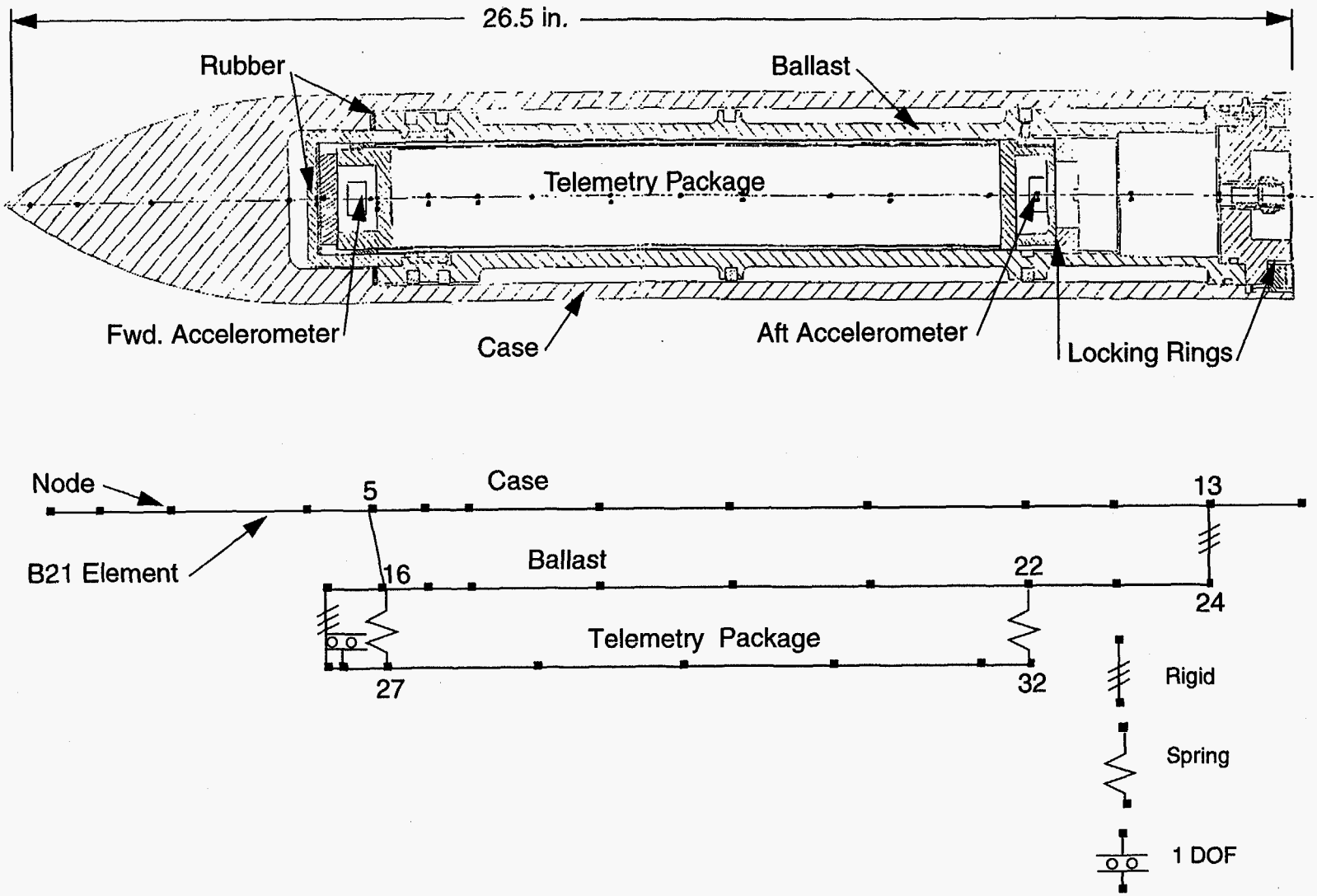

Figure 2. Structural Model of MOU Penetrator with Connections Between the Case, Ballast and Telemetry Package

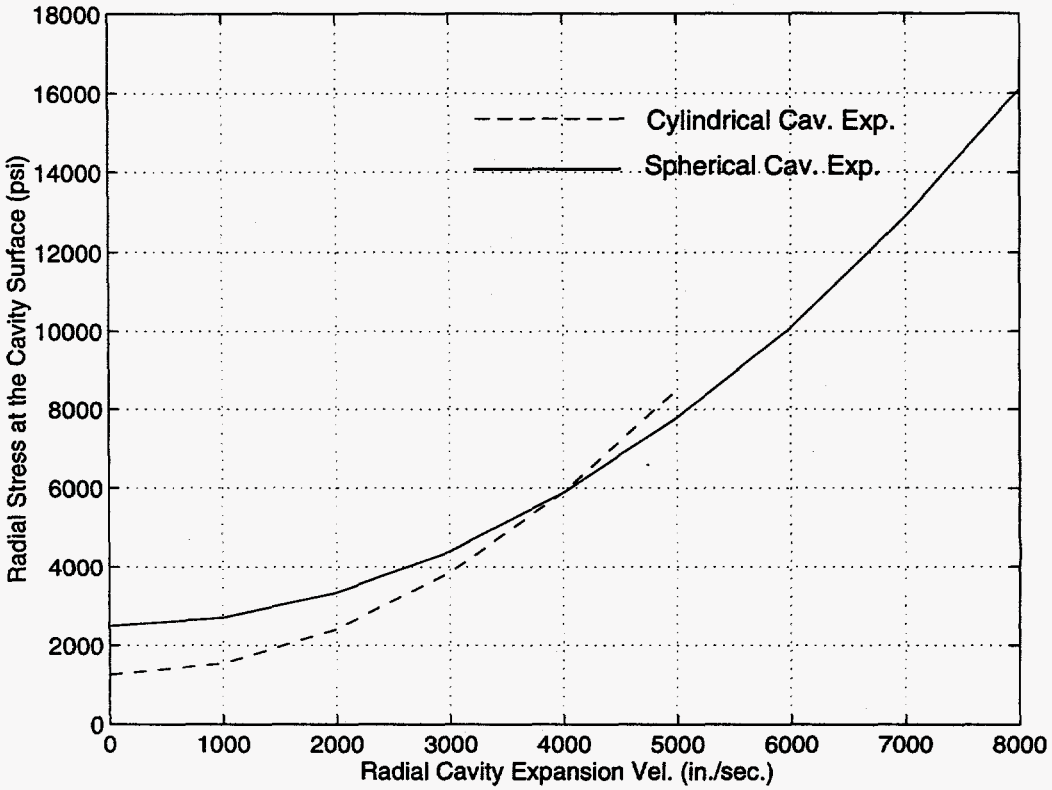

Figure 3. Radial Stress at the Spherical or Cylindrical Cavity Surface versus Cavity Expansion Velocity in Antelope Dry Lake Soil

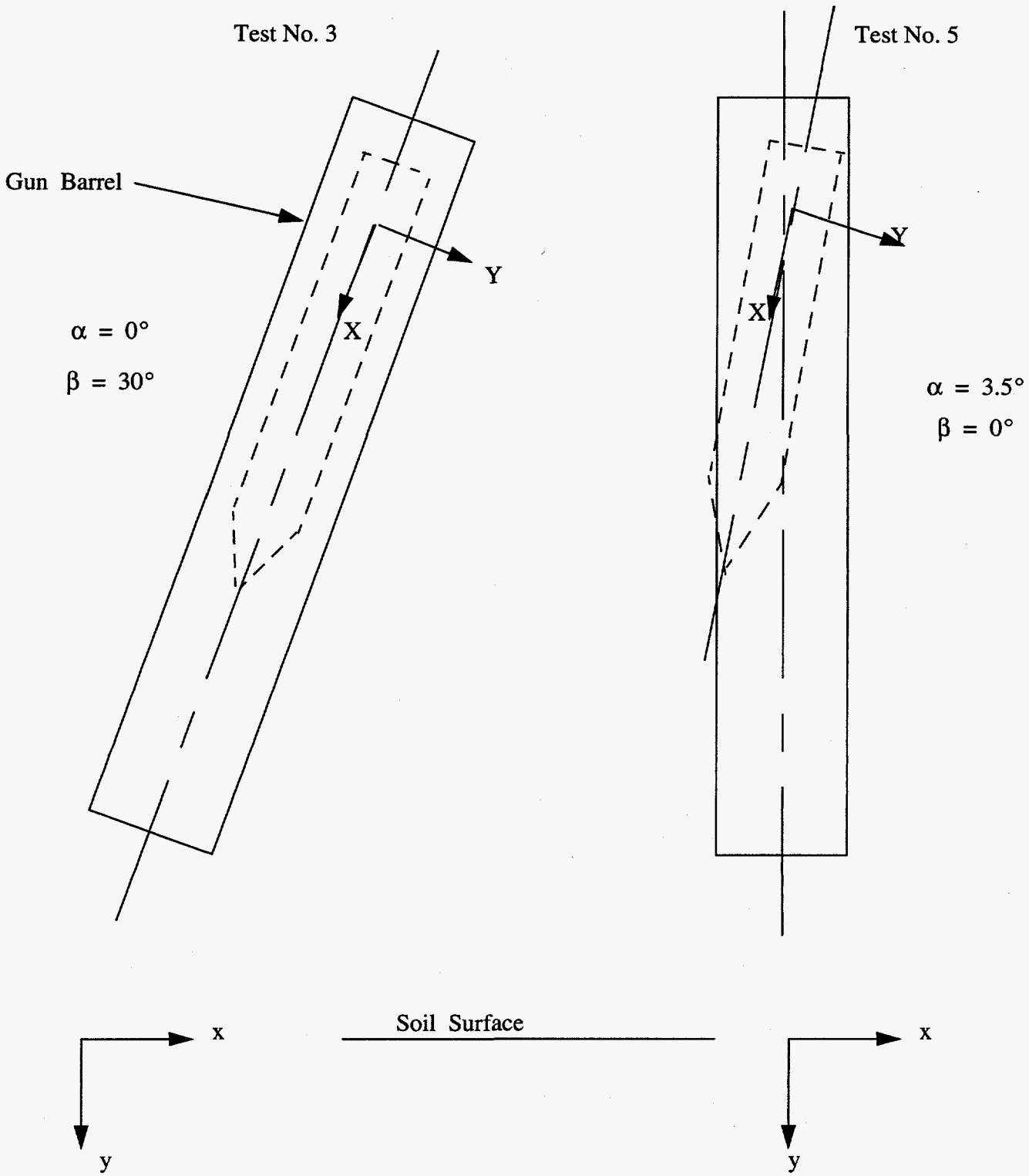

x, y ABAQUS global coordinates

X, Y Coordinates fixed in penetrator

Figure 4. Orientation of Gun and Penetrator in Oblique Penetration Tests into Antelope Dry Lake

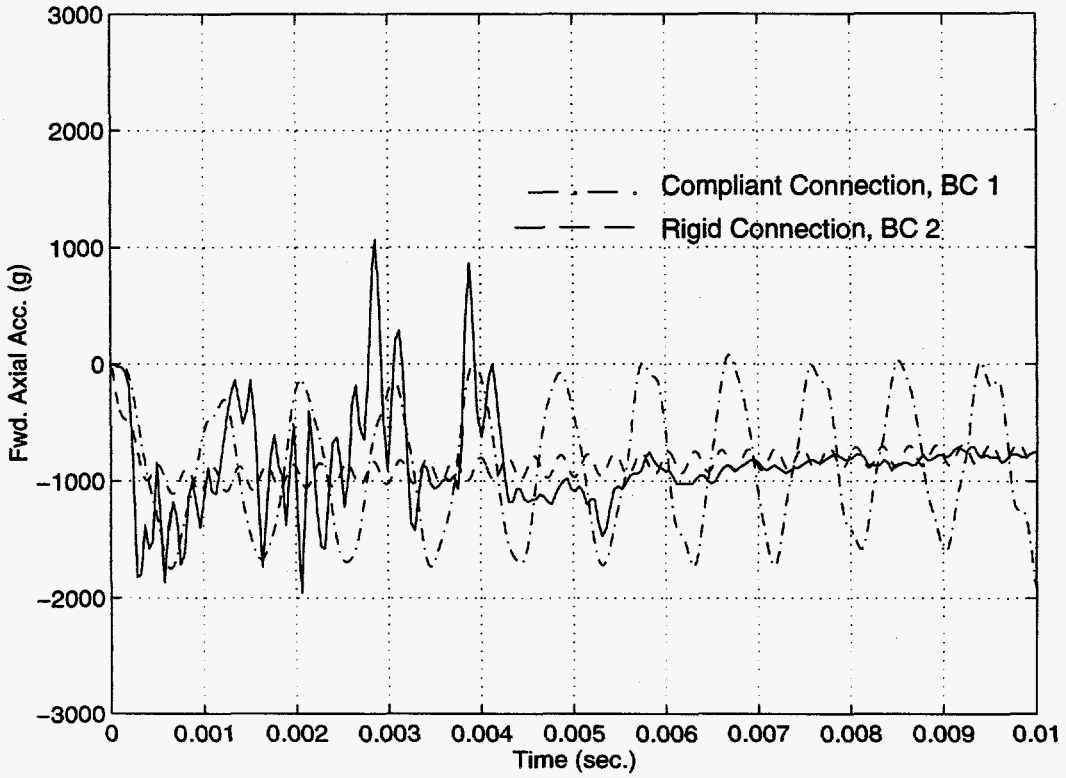

(a)

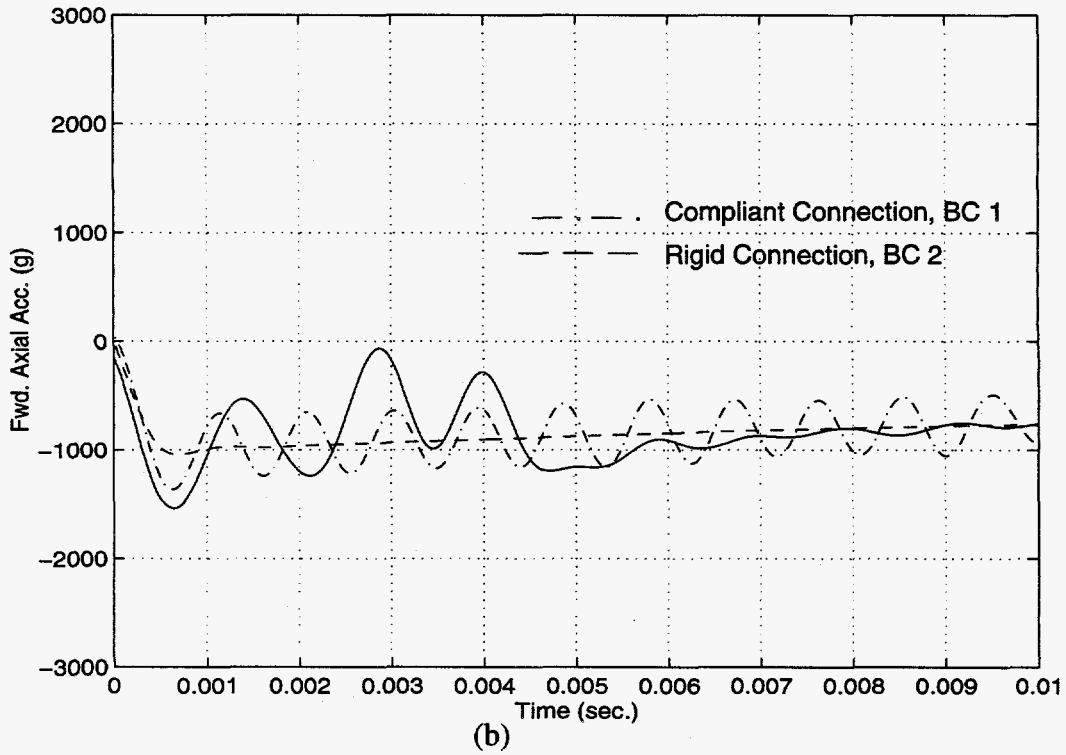

(b)

Figure 5. Axial Acceleration at Forward Accelerometer in Test No. 3 after Filtering with 3,500 Hz Low-Pass Filter (a) and 1,000 Hz Low-Pass Filter (b)

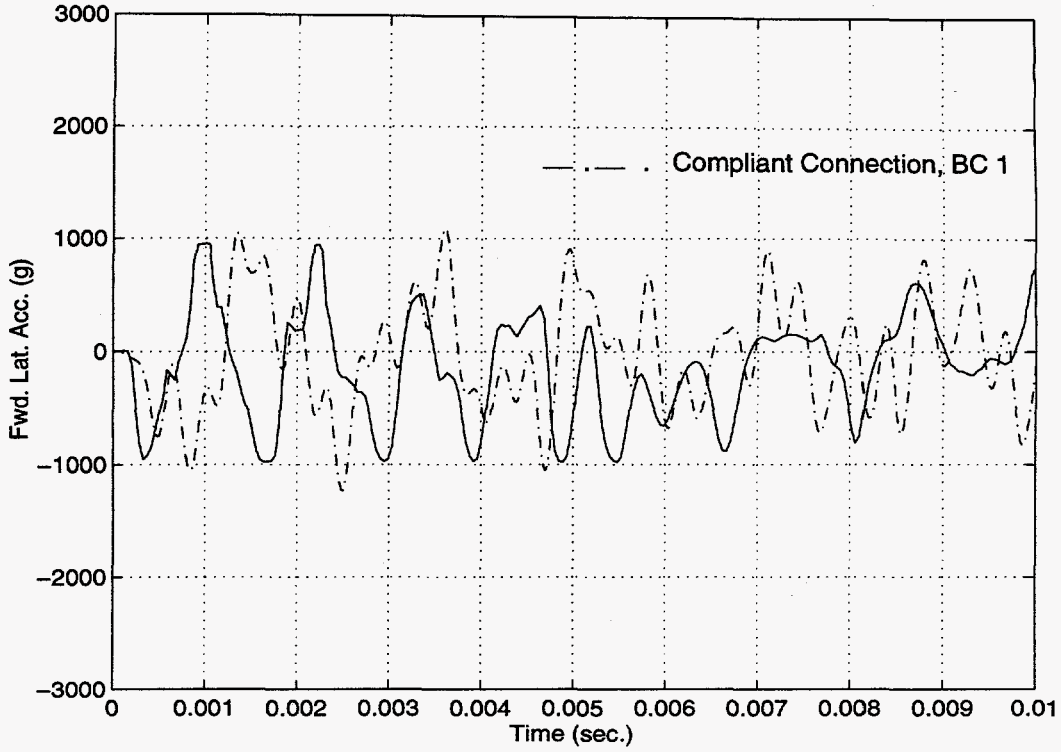

(a)

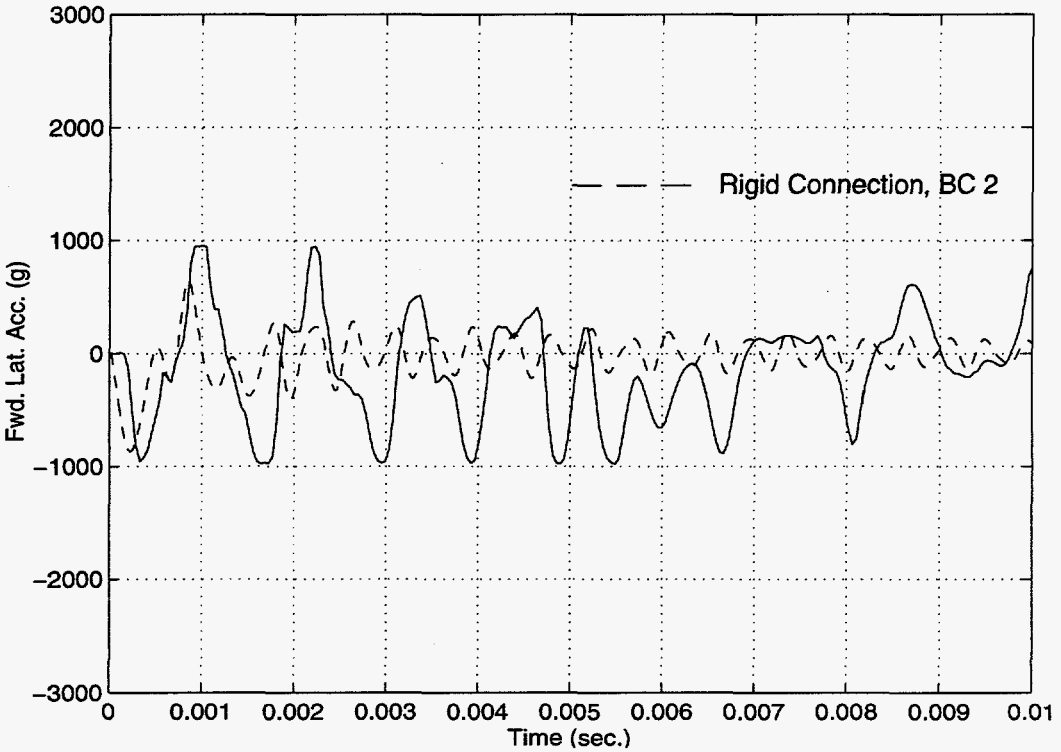

(b)

Figure 6. Lateral Acceleration at Forward Accelerometer in Test No. 3 for Compliant (a) and Rigid (b) Restraint Connections

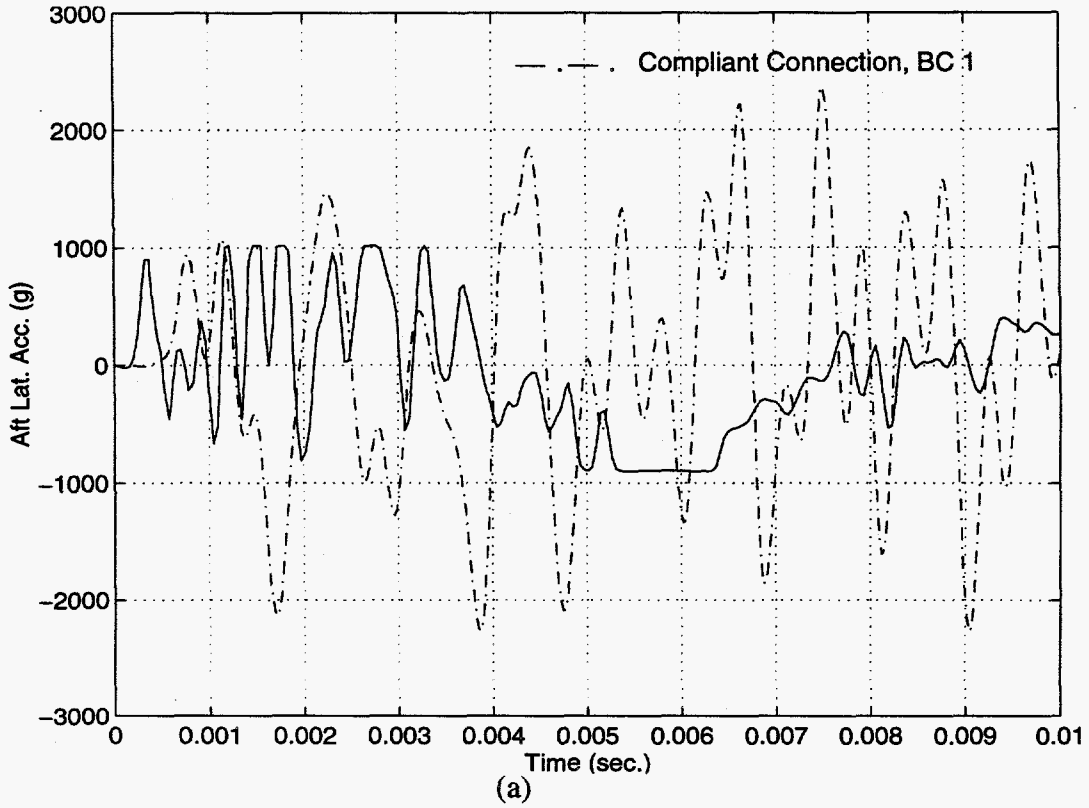

(a)

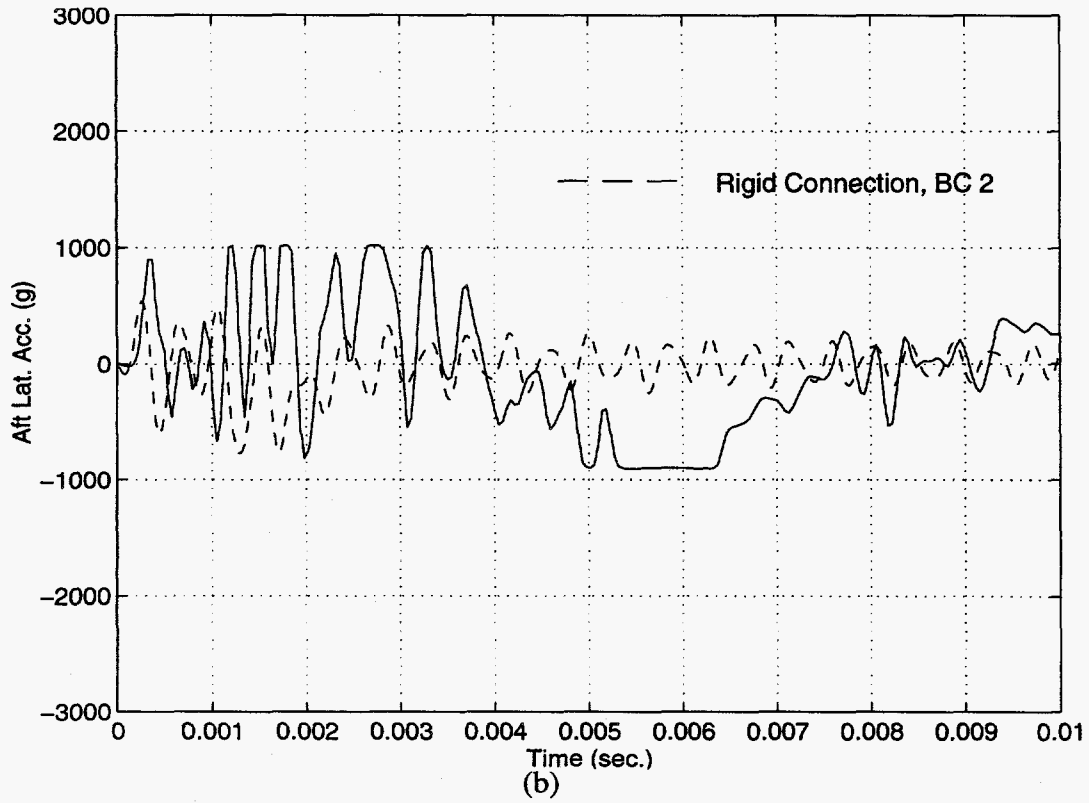

(b)

Figure 7. Lateral Acceleration at Aft Accelerometer Location in Test No. 3 for Compliant (a) and Rigid (b) Restraint Connections

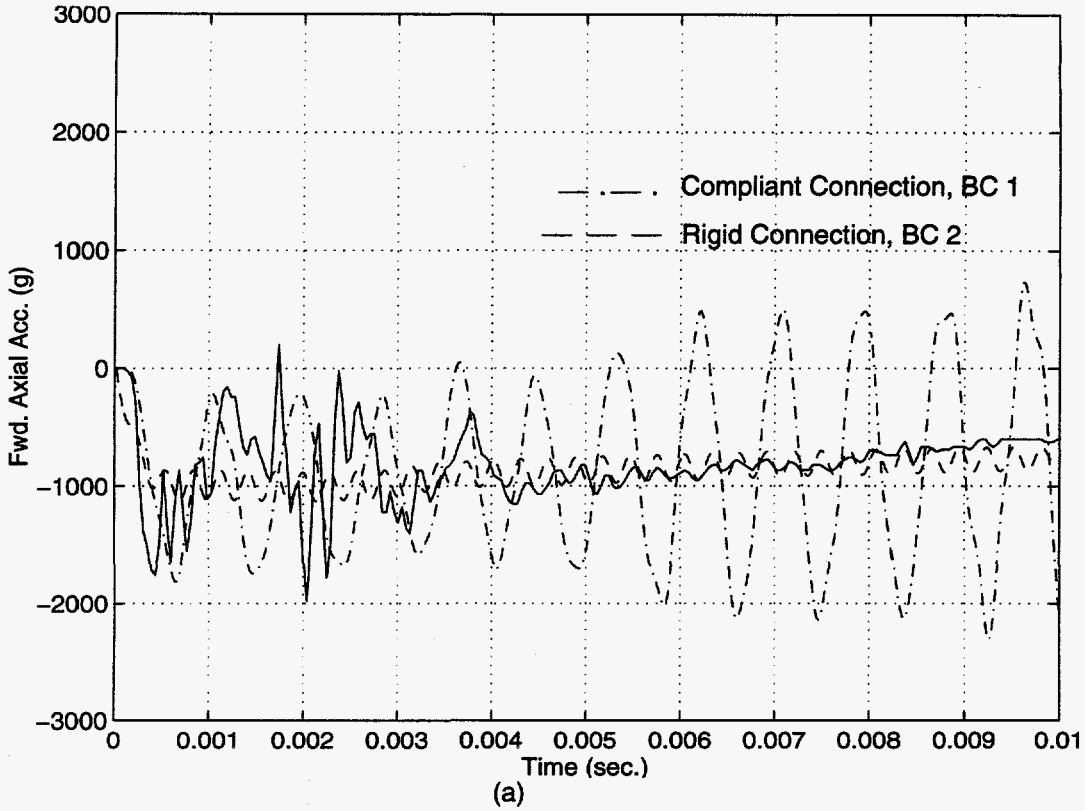

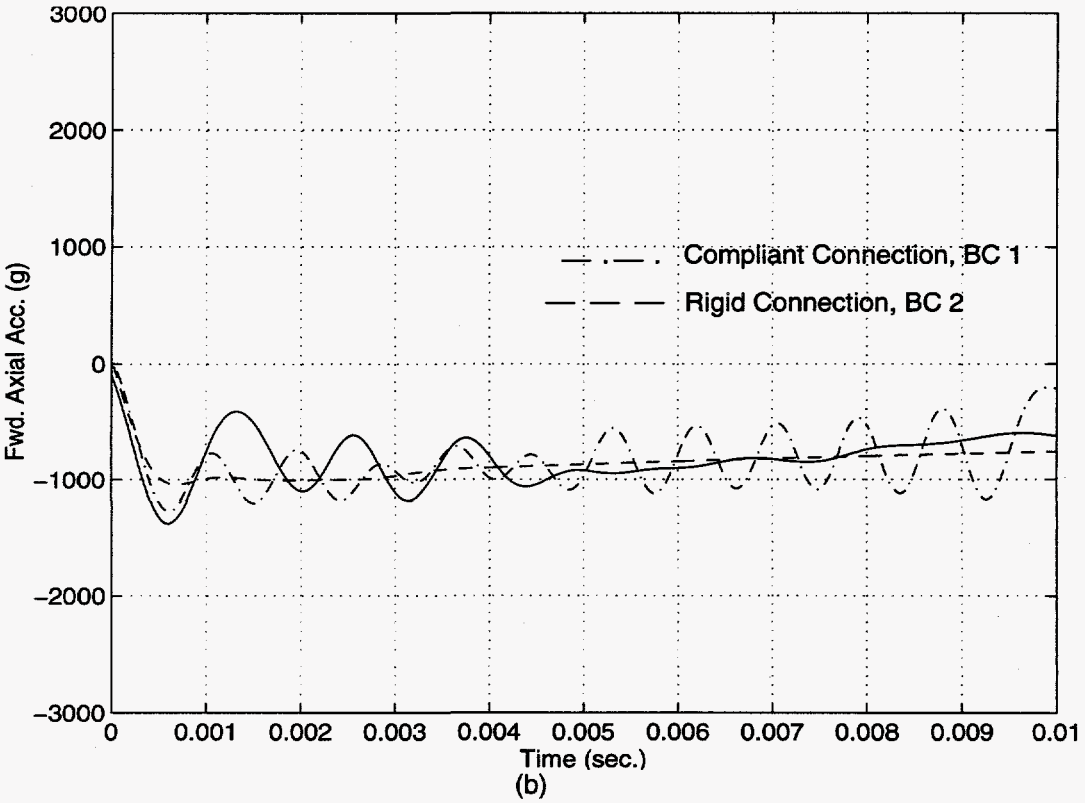

Figure 8. Axial Acceleration at Forward Accelerometer in Test No. 5 after Filtering with 3,500 Hz Low-Pass Filter (a) and 1,000 Hz Low-Pass Filter (b)

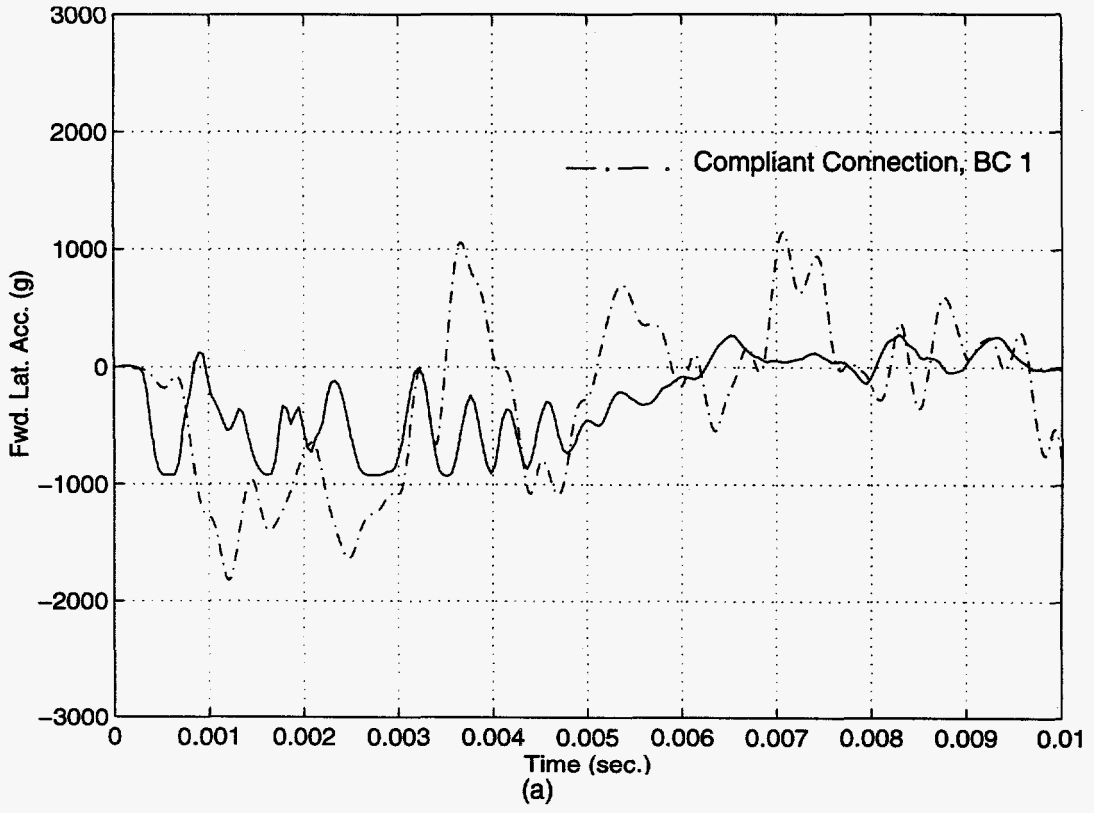

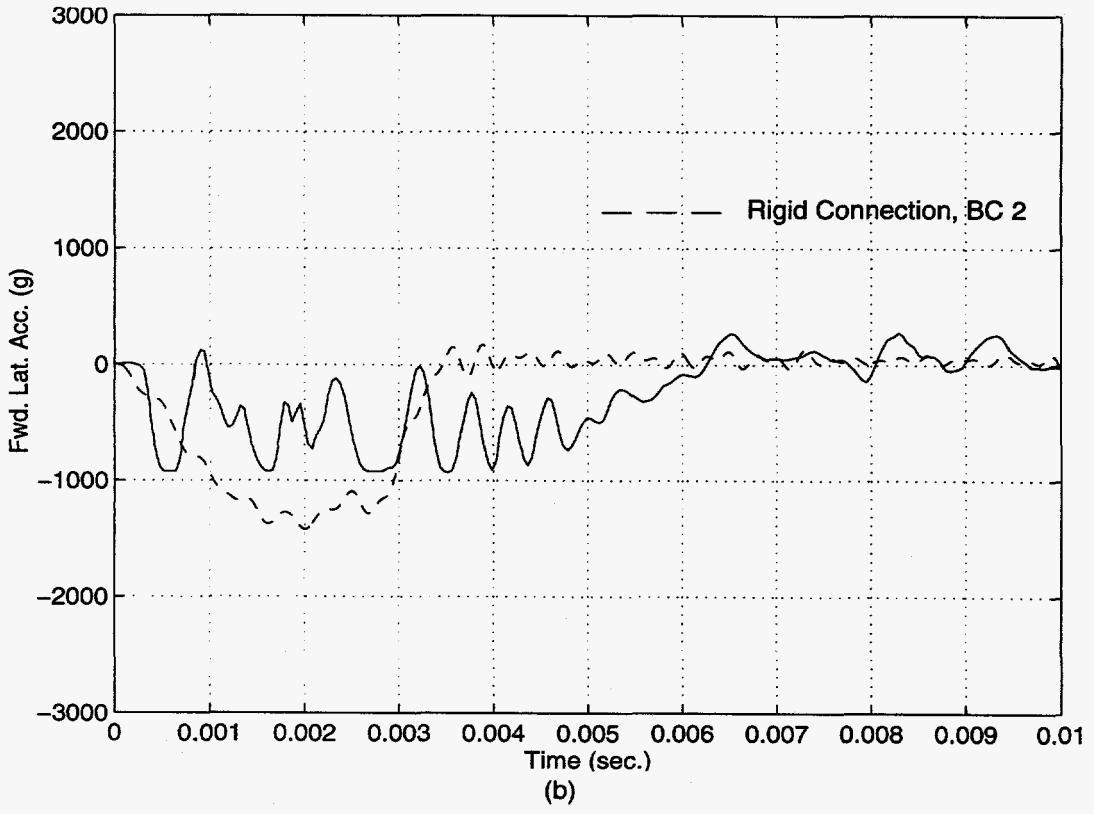

Figure 9. Lateral Acceleration at Forward Accelerometer in Test No. 5 for Compliant (a) and Rigid (b) Restraint Connections

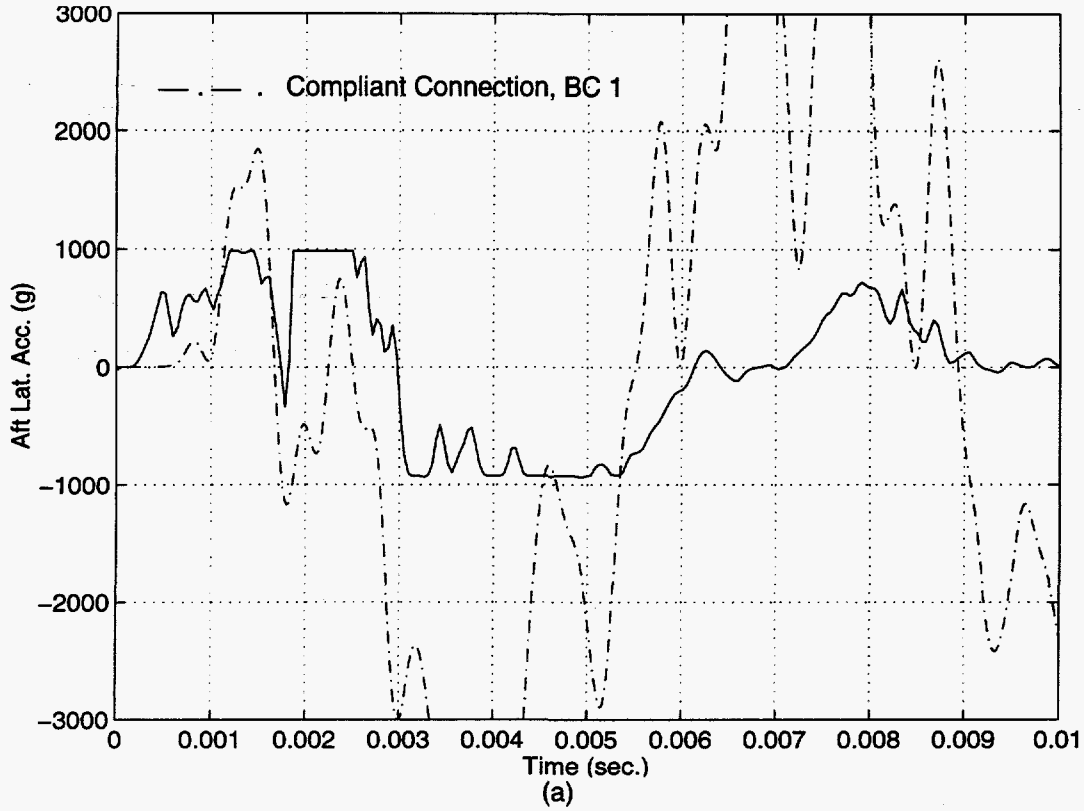

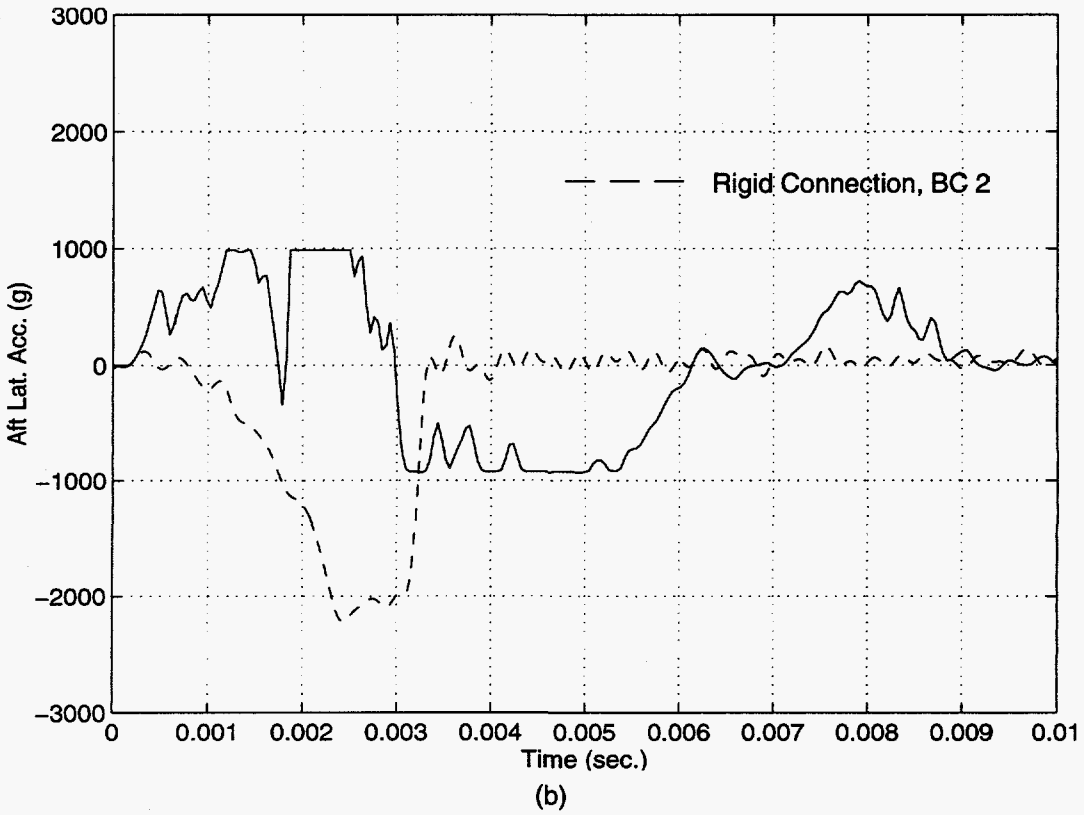

Figure 10. Lateral Acceleration at Aft Accelerometer Location in Test No. 5 for Compliant (a) and Rigid (b) Restraint Connections

DISTRIBUTION:

2 Applied Research Associates, Inc.
Attn: Wayne Young
Peter Dunn
4300 San Mateo Blvd., N.E.
Suite A220
Albuquerque, NM 87110

1 HQ/DNA/SPSD
Defense Nuclear Agency
Attn: Mike Giltrud
6801 Telegraph Road
Alexandria, VA 22310-3398

1 Lawrence Livermore National Lab
Attn: Francois Heuze
P. O. Box 808, L-200
Livermore, CA 94550

1 Lawrence Livermore National Lab
Attn: Albert Holt
P. O. Box 808, L-163
Livermore, CA 94550

2 Waterways Experiment Station
Geomechanics and Explosion Effects
Attn: Mark Adley
J. Donald Cargile
3909 Halls Ferry Road
Vicksburg, MS 39180-6199

1 Wright Lab Armament Directorate
WL/MNMW
Attn: Dr. Joseph Foster Jr.
101 W. Eglin Blvd., Ste 239
Eglin AFB, FL 32542-6810

1 MS0427 W. R. Reynolds, 2103
1 MS0453 D. L. McCoy, 2104
1 MS0483 N. R. Hansen, 2165
1 MS0303 M. J. Forrestal, 2411
1 MS0303 R. G. Lundgren, 2411
1 MS0987 R. J. Franco, 2664
1 MS0987 D. E. Ryerson, 2664
1 MS0986 M. R. Platzbecker, 2665
1 MS0437 R. K. Thomas, 9118
1 MS0841 P. J. Hommert, 9100

DISTRIBUTION: (Cont.)

1	MS0443	H. S. Morgan, 9117
1	MS0437	E. P. Chen, 9118
1	MS0321	W. J. Camp, 9200
1	MS0820	P. Yarrington, 9232
1	MS0439	D. R. Martinez, 9234
10	MS0439	D. B. Longcope, 9234
1	MS0555	V. I. Bateman, 9742
1	MS9018	Central Tech Files, 8523-2
5	MS0899	Technical Library, 4414
2	MS0619	Review & Approval Desk, 12630 For DOE/OSTI